THERMAL MODELING OF MULTI-SHAPE HEATING SOURCES ON N-LAYER ELECTRONIC BOARD

by

Eric MONIER-VINARD[a]*, Minh-Nhat NGUYEN[b], Najib LARAQI[b], and Valentin BISSUEL[a]

[a] Thales Global Services, Velizy-Villacoublay, France
[b] LTIE, Paris West University, Ville d'Avray, France

Original scientific paper
https://doi.org/10.2298/TSCI160416300M

The present work completes the toolbox of analytical solutions that deal with resolving steady-state temperatures of a multi-layered structure heated by one or many heat sources. The problematic of heating sources having non-rectangular shapes is addressed to enlarge the capability of analytical approaches. Moreover, various heating sources could be located on the external surfaces of the sandwiched layers as well as embedded at interface of its constitutive layers.
To demonstrate its relevance, the updated analytical solution has been compared with numerical simulations on the case of a multi-layered electronic board submitted to a set of heating source configurations. The comparison shows a high agreement between analytical and numerical calculations to predict the centroid and average temperatures.
The promoted analytical approach establishes a kit of practical expressions, easy to implement, which would be cumulated, using superposition principle, to help electronic designers to early detect component or board temperatures beyond manufacturer limit.
The ability to eliminate bad concept candidates with a minimum of set-up, relevant assumptions and low computation time can be easily achieved.

Key words: *analytical thermal modeling, multi-layer printed circuit board, multi-shape heating sources*

Introduction

More than ever, electronic board designers have to deal today with constraining powered devices on high density electronic boards. The miniaturization of electronic component is reinforcing the need to simulate in thinner details its surrounding board architecture in order to manage its contribution to the heat transfer.

If numerical simulation methods are mandatory to find the appropriate power dissipation of many components on an electronic board, the sensitivity of the components temperatures to early conception changes is today a crucial concern. Moreover, numerical approaches can be often cumbersome, expensive and hard to assess by none-expert which are not familiar with theirs calculation rules. So it seems much convenient to develop a more comprehensible approach allowing designers to early estimate the critical temperatures of electronic compo-

* Corresponding author, e-mail: eric.monier-vinard@thalesgroup.com

nents. There are numerous works in the literature based on an analytical approach which deal with the problematic of electronic component cooling.

Thus, an analytic method for predicting the temperature distribution over a printed circuit board (PCB) is presented in [1]. The model assumes that the n-layer structure of a board can be represented by a single layer using effective thermal conductivities approach. Ellison [2] proposed a way to take into account two-resistance thermal networks representing the electronic component thermal behavior.

Chien *et al.* [3] established a temperature solution of a five-layer substrate for an electronic chip. The authors used circular embedded heating source in order to reduce computation time. Thus the solution is in the form of a single integration rather than double Fourier integration mandatory for square or rectangular heating source.

Rinaldi [4] applies the generalized image method to model the thermal resistance of a multilayer substrate submitted to an embedded planar or volume heating source. Albers [5] proposed a recursion relationship which was derived from the *n*-layer electrical problem and is applicable to solve the multilayer steady-state heat equation of a rectangular heating source cooled by an infinite heat sink. More recently Bagnall *et al.* [6] supplied a 3-D steady-state solution for a heat source embedded in a multi-layer substrate based on Fourier series solution and recursive relations.

Culham *et al.* [7] solved the 3-D Fourier series solution for a multi-layer substrate having its four sides subject to a uniform Fourier-type boundary conduction to address the thermal characterization of electronic packages.

Ditri [8] developed a useful form to consider the case of a set of *N* similar rectangular heating micro sized sources spaced with a regular pitch for multi-fingered power transistors. Vintrou *et al.* [9] extended the approach to address the transient regime for a multi-layered chip structure. The impact of a large set of complex source shapes on the thermal spreading resistance has been summarized by Sadeghi *et al.* [10]. Other analytical approaches based on the integral-balance method was suggested to solve linear and non-linear heat conduction problems [11, 12]

Maranzana *et al.* [13] and Pailhes *et al.* [14] dealt with the quadrupole method to assemble pyramidal multi-block or multi-layered slabs with internal heating sources.

Based on these theoretical studies, a set of analytical models was derived [15, 16] to address the thermal design of multi-layered PCB with multi-sources mounted on its external surfaces in order to assist designers in fulfilling their practical needs.

The purpose of the current work is to extend that model by now considering the modeling of new source shapes.

Initial status of the analytical approach

The established analytical formulation allows a fast evaluation of the temperature profile of a set of constitutive cross-plane dielectric or conductive layers according with the following capabilities:

– quantification of steady-state temperatures of superposed multiple sources,
– limited to rectangular or square board shape,
– consideration of orthotropic thermal conductivities,
– Fourier-type (3rd) boundary condition on external upper and lower surfaces,
– moreover, the uniform heat transfer coefficient of the external upper and lower surfaces can be minimized (*e. g.* 10^{-9}) or maximized (*e. g.* 10^{9}) to cover Dirichlet-type (1st) or Neumann-type (2nd) kinds of boundary conditions on external plane surface,
– Neumann-type (2nd) boundary condition on the layer lateral sides,

– assumption of perfect interlayer contact,
– restricted to rectangular or square heating source shapes, and
– heating source located on any layer or between two layers.

The analytical modeling of the various source shapes is henceforth our concern:

– extension to circular or annular source shapes,
– extension to isosceles triangular shape, and
– consideration of square sources rotated 45 degree.

Analytical model and assumptions

The proposed analytical formulation allows a fast evaluation of the temperature profile of a set of constitutive dielectric or conductive layers under steady-state conditions.

The electronic board is cooled from its top and rear surfaces to the ambient by coupled convection and radiation heat exchanges to enable potential infrared measurement validation at laboratory boundary conditions. Both surfaces are exposed to a specific uniform heat transfer coefficient, named, respectively, *ht* and *hr*.

The board shape is always approximated by a rectangular or a square geometry. Its overall length, *Lb*, width, *Wb*, and thickness, *Hb*, are depicted in fig. 1.

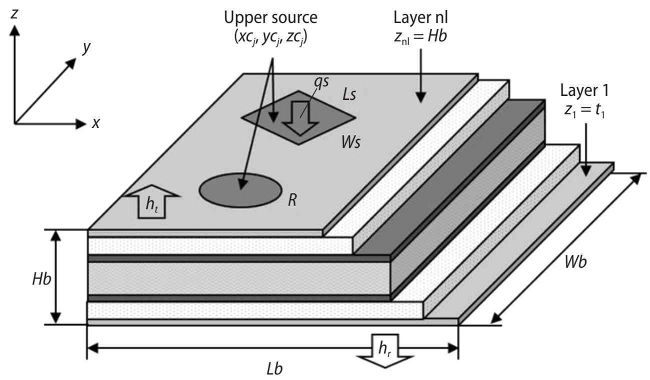

Figure 1. Definition of geometric parameters of the analytical model

The generalized steady-state governing equation used for this study is the Laplace equation. Thus, the governing equation applied to an orthotropic layer called *i*, is:

$$Kx_i \frac{\partial^2 \theta_i(x,y,z)}{\partial x^2} + Ky_i \frac{\partial^2 \theta_i(x,y,z)}{\partial y^2} + Kz_i \frac{\partial^2 \theta_i(x,y,z)}{\partial z^2} = 0 \quad \text{for} \quad i = 1,\ nl \tag{1}$$

The subscript x, y, z are Cartesian co-ordinates, $\theta_i(x, y, z) = T_i(x, y, z) - T_\infty$ is the difference between the local temperature in layer *i* and the reference temperature.

Lateral edges are assumed to be adiabatic due to their small thickness compared with the other dimensions of the board:

$$Kx_i \left.\frac{\partial \theta_i(x,y,z)}{\partial x}\right|_{x=0,\,Lb} = Ky_i \left.\frac{\partial \theta_i(x,y,z)}{\partial y}\right|_{y=0,\,Wb} = 0 \qquad \text{for} \quad i = 1,\ nl \tag{2}$$

A planar heating source can be located between two adjacent layers as well as on board external surfaces. Its heat flow rates q is assumed uniform over the source.

Thus, the different types of boundary condition will be used depending on source location.

If the heating source is located on the top surface ($z = Hb$ and $0 \le x \le Lb$ and $0 \le y \le Wb$):

$$-Kz_{nl}\left.\frac{\partial\theta_{nl}(x,y,z)}{\partial z}\right|_{z=Hb}=ht\theta_{nl}(x,y,Hb)-u(x,y)\quad\text{and}$$
$$-Kz_1\left.\frac{\partial\theta_1(x,y,z)}{\partial z}\right|_{z=0}=-hr\theta_1(x,y,0)\tag{3}$$

If the heating source is located on the rear surface ($z = 0$ and $0 \le x \le Lb$ and $0 \le y \le Wb$):

$$-Kz_1\left.\frac{\partial\theta_1(x,y,z)}{\partial z}\right|_{z=0}=-hr\theta_1(x,y,0)+r(x,y)\quad\text{and}$$
$$-Kz_{nl}\left.\frac{\partial\theta_{nl}(x,y,z)}{\partial z}\right|_{z=Hb}=ht\theta_{nl}(x,y,Hb)\tag{4}$$

If the heating source is embedded between two adjacent layers ($z = z_i$ and $0 \le x \le Lb$ and $0 \le y \le Wb$):

$$Kz_{i+1}\left.\frac{\partial\theta_{i+1}(x,y,z)}{\partial z}\right|_{z=z_i}-Kz_i\left.\frac{\partial\theta_i(x,y,z)}{\partial z}\right|_{z=z_i}=e(x,y)\quad\text{for}\quad i=1,\ nl-1\tag{5}$$

Each interface of adjacent layer is considered in perfect thermal contact. Thus, inter-layer temperature and flux continuity boundary conditions ($0 \le x \le Lb$ and $0 \le y \le Wb$) have to be satisfied:

$$\left.\theta_{i+1}(x,y,z)\right|_{z=z_i}=\left.\theta_i(x,y,z)\right|_{z=z_i}\quad\text{for}\quad i=1,\ nl-1\tag{6}$$

$$Kz_{i+1}\left.\frac{\partial\theta_{i+1}(x,y,z)}{\partial z}\right|_{z=z_i}-Kz_i\left.\frac{\partial\theta_i(x,y,z)}{\partial z}\right|_{z=z_i}=0\quad\text{for}\quad i=1,\ nl-1\tag{7}$$

The 3-D temperature distribution of a PCB has been solved using conventional Fourier series. The final practical solution of the temperature distribution can be written:

$$\theta(x,y,z)=\sum_{j=1}^{ns}\frac{4\left.qs\right|_{zc\,j}}{Sb}\sum_{m=0}^{M_j}\sum_{n=0}^{N_j}\frac{A_{m,j}B_{n,j}}{(\delta_m+1)(\delta_n+1)}\cos\left(\frac{m\pi}{Lb}x\right)\cos\left(\frac{n\pi}{Wb}y\right)\left.\omega_{m,n}(z)\right|_{zc_j}\tag{8}$$

The upper limit M_j and N_j of the truncated Fourier series depend on accuracy requirements and m and n are non-negative integers. In practice, the number of terms in the double summation is based on a ratio proportional to a board-source size which has to be multiply per an appropriate factor, named a. A high agreement is achieved when that parameter is fixed to 15 [16].

The Kronecker function, δ, is brought to extend the domain validity to the indeterminate cases when m and/or n are equal to zero. The mean temperature is obtained by integrating both cosine functions over the source region.

$$\bar{\theta}_k=\sum_{j=1}^{ns}\frac{4\left.qs\right|_{zc\,j}}{Sb\cdot Ss_k}\sum_{m=0}^{M}\sum_{n=0}^{N}\frac{A_{m,j}B_{n,j}\overline{A_{m,k}}\,\overline{B_{n,k}}}{(\delta_m+1)(\delta_n+1)}\left.\omega_{m,n}(zc_k)\right|_{zc_j}\tag{9}$$

The parameters Sb and Ss_k are, respectively, the areas of the board and of the ns heating sources.

The expression $\omega_{m,n}(zc_k)|_{zc_j}$ is the z-axis thermal profile depending on the position of the heating source in the layers.

The $A_{m,j}B_{n,j}$ and $\overline{A_{m,k}\,B_{m,k}}$ are, respectively, local and average Fourier coefficients, depending on the shape of the source.

Multiple cross-plane heating source

The z-axis thermal profile $\omega_{m,n,i}(z)$, over the cross-section, depends on the number of layers which are to be scrutinized to properly characterize the thermal behavior of the board. Its definition according to the boundary conditions (3), (4), or (5) is:

– heating source on the upper board surface: $zc_j = Hb \rightarrow \omega_{m,n}(z)|_{zc_j} = \omega u_{m,n,i}(z)$ with $i \rightarrow z_{i-1} \le z \le z_i$

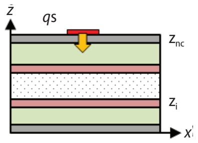

$$\omega u_{m,n,i}(z) = \frac{Nu_{m,n,i}}{Du_{m,n,i}}\left[\omega c_{m,n,i}(z - z_{i-1}) + \frac{\chi u_{m,n,i}}{Kz_i}\omega s_{m,n,i}(z - z_{i-1})\right]\mathrm{e}^{(z-Hb)r_{m,n,i}} \quad (10)$$

– heating source on the rear board surface: $zc_j = 0 \rightarrow \omega_{m,n}(z)|_{zc_j} = \omega r_{m,n,i}(z)$ with $i \rightarrow z_{i-1} \le z \le z_i$

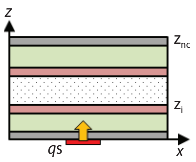

$$\omega r_{m,n,i}(z) = \frac{Nr_{m,n,i}}{Dr_{m,n,i}}\left[\omega c_{m,n,i}(z_i - z) + \frac{\chi r_{m,n,i}}{Kz_i}\omega s_{m,n,i}(z_i - z)\right]\mathrm{e}^{-(z+Hb)r_{m,n,i}} \quad (11)$$

– heating source at the interface of the s and $s + 1$ layers: $0 < zc_j < Hb \rightarrow \omega_{m,n}(z)|_{zc_j} = \omega e_{m,n,i}(z)$

– $0 \le z \le z_s$ with $i \rightarrow z_{i-1} \le z \le z_i$:

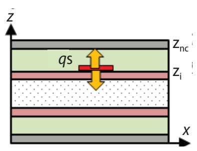

$$\omega e_{m,n,i}(z) = \frac{Ner_{m,n,i}}{Der_{m,n,i}}\left[\omega c_{m,n,i}(z - z_{i-1}) + \frac{\chi u_{m,n,i}}{Kz_i}\omega s_{m,n,i}(z - z_{i-1})\right]\cdot$$
$$\cdot\mathrm{e}^{(z-Hb)r_{m,n,i}} \quad (12)$$

– $z_s \le z \le Hb$ with $i \rightarrow z_{i-1} \le z \le z_i$:

$$\omega e_{m,n,i}(z) = \frac{Neu_{m,n,i}}{Deu_{m,n,i}}\left[\omega c_{m,n,i}(z_i - z) + \frac{\chi r_{m,n,i}}{Kz_i}\omega s_{m,n,i}(z_i - z)\right]\mathrm{e}^{-(z+Hb)r_{m,n,i}}$$

The formulae of $\chi u_{m,n,i}$ and $\chi r_{m,n,i}$ functions are given by the recursive relationships:

$$\begin{cases} i = 1 \quad \Rightarrow \quad \chi u_{m,n,1} = hr \\ 1 \le i < nl \quad \Rightarrow \quad \chi u_{m,n,i+1} = \dfrac{\alpha_{m,n,i} + \chi u_{m,n,i}\,\gamma_{m,n,i}}{\gamma_{m,n,i} + \chi u_{m,n,i}\,\beta_{m,n,i}} \end{cases} \quad (13)$$

$$\begin{cases} i = nl \quad \Rightarrow \quad \chi r_{m,n,nl} = ht \\ 1 \le i < nl \quad \Rightarrow \quad \chi r_{m,n,i} = \dfrac{\alpha_{m,n,i+1} + \chi r_{m,n,i+1}\,\gamma_{m,n,i+1}}{\gamma_{m,n,i+1} + \chi r_{m,n,i+1}\,\beta_{m,n,i+1}} \end{cases} \quad (14)$$

While the others parameters of the solution are presented in Appendix A.

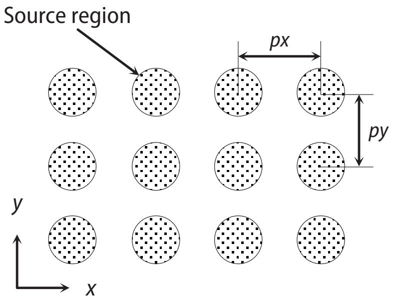

Figure 2. Matrix form of a set of identical heating sources

Multiple similar active heating sources

The calculation of the temperature distribution of a set of heating sources can be optimized if these ones have the same dimension, the same dissipation, and are arranged in a pattern, as shown in fig. 2.

Instead of applying the superposition principle, the matrix source expression allows to minimize the computing time:

$$\theta(x,y,z) = \frac{4qs|_{zc}}{Sb}\sum_{m=0}^{M}\sum_{n=0}^{N} C_{m,n}\frac{A_m B_n}{(\delta_m+1)(\delta_n+1)}\cdot \\ \cdot\cos\left(\frac{m\pi}{Lb}x\right)\cos\left(\frac{n\pi}{Wb}y\right)\omega_{m,n}(z)\Big|_{zc} \tag{15}$$

where

$$C_{m,n} = \left[\frac{\sin\left(\frac{m\pi}{Lb}\frac{px}{2}nsx\right)}{\sin\left(\frac{m\pi}{Lb}\frac{px}{2}\right)+\delta_m} + nsx\delta_m\right]\left[\frac{\sin\left(\frac{n\pi}{Wb}\frac{py}{2}nsy\right)}{\sin\left(\frac{n\pi}{Wb}\frac{py}{2}\right)+\delta_n} + nsy\delta_n\right]$$

The parameters px and py are axial pitches of two heating sources according to the x- and y-direction, respectively.

The parameters nsx and nsy are the source number according to the x- and y-direction, respectively.

Multi-shape heating source

By applying the classical orthogonality principle on the boundary conditions (3), (4), and (6), the Fourier coefficients $A_{m,j}{\cdot}B_{n,j}$ can be deducted from the following expression:

$$A_{m,j}B_{n,j} = \iint_{Ss_j}\cos\left(\frac{m\pi}{Lb}x\right)\cos\left(\frac{n\pi}{Wb}y\right)\mathrm{d}x\mathrm{d}y \tag{16}$$

Thus, the Fourier coefficients $A_{m,j}B_{n,j}$ derived for different source shapes are defined in tab. 1.

The rhombus parameters are used to treat the case when a square source is rotated 45 degree but two opposite isosceles triangle could be convenient as well. The Bessel's form of the circular shape case, eq. (18), is based on Laraqi study [17] of the thermal resistance of random contacts on a semi-infinite substrate. Thus equation is derived by the development of the multiple integral (12) over the circular domain of heating source as shown in the Appendix B.

Calculation corner

Mathcad® software version 15.0 was used to conduct the analytical model calculations. Its results are reported in the next tables by the subscript AM, for analytical model calculation. The analytical results are compared to the computation ones given by an Ansys© electronic cooling software named Icepak©. The subscript NM for numerical model designs its results.

Table 1. Practical glossary for multiple heating source shapes

Name	Geometry reference	Fourier coefficients A_mB_n	
Rectangular or square shapes	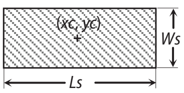	$A_{m,j}B_{n,j} = Ss_j \cos\left(\frac{m\pi}{Lb}xc_j\right)\cos\left(\frac{n\pi}{Wb}yc_j\right)\cdot$ $\cdot\operatorname{sinc}\left(\frac{m\pi}{Lb}\frac{Ls_j}{2}\right)\operatorname{sinc}\left(\frac{n\pi}{Wb}\frac{Ws_j}{2}\right)$ where (Ls_j, Ws_j) are, respectively, length and width of the source number j and (xc_j, yc_j) are its center co-ordinates	(17)
Circular shape	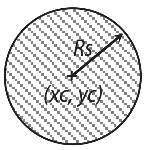	$A_{m,j}B_{n,j} = Ss_j \cos\left(\frac{m\pi}{Lb}xc_j\right)\cos\left(\frac{n\pi}{Wb}yc_j\right)f(R_j)$ where $f(R_j) = J_2\left[R_j\sqrt{\left(\frac{m\pi}{Lb}\right)^2+\left(\frac{n\pi}{Wb}\right)^2}\right] + J_0\left[R_j\sqrt{\left(\frac{m\pi}{Lb}\right)^2+\left(\frac{n\pi}{Wb}\right)^2}\right]$ where R_j is the radius of the source number j, xc_j and yc_j are its center location, and J_2 and J_o are the Bessel functions of the first order	(18)
Annular shape	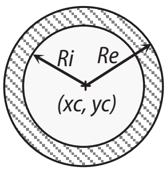	$A_{m,j}B_{n,j} = \cos\left(\frac{m\pi}{Lb}xc_j\right)\cos\left(\frac{n\pi}{Wb}yc_j\right)\left[Ss_{e,j}f(Re_j) - Ss_{i,j}f(Ri_j)\right]$ where Ri_j, Re_j are, respectively, interior and exterior radius of the source number j and (xc_j, yc_j) are its center location	(19)
Rhombus	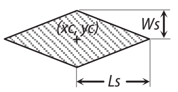	$A_{m,j}B_{n,j} = Ss_j \cos\left(\frac{m\pi}{Lb}xc_j\right)\cos\left(\frac{n\pi}{Wb}yc_j\right)\sin c\left(\kappa_{m,n,j}\right)\sin c\left(\xi_{m,n,j}\right)$ where $\kappa_{m,n,j} = \frac{m\pi}{Lb}\frac{Ls_j}{2} + \frac{n\pi}{Wb}\frac{Ws_j}{2}$ and $\xi_{m,n,j} = \frac{m\pi}{Lb}\frac{Ls_j}{2} - \frac{n\pi}{Wb}\frac{Ws_j}{2}$	(20)
Isosceles triangle	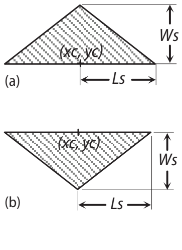	$A_{m,j}B_{n,j} = f_{m,n,j} + sg_j g_{m,n,j} - sg_j h_{m,n,j}$ where $f_{m,n,j} = Ss_j \cos\left(\frac{m\pi}{Lb}xc_j\right)\cos\left(\frac{n\pi}{Wb}yc_j\right)\sin c\left(\kappa_{m,n,j}\right)\sin c\left(\xi_{m,n,j}\right)$ $g_{m,n,j} = Ss_j\frac{yc_j}{Ws_j}\cos\left(\frac{m\pi}{Lb}xc_j\right)\sin c\left(\frac{n\pi}{Wb}yc_j\right)\cdot$ $\cdot\left[\sin c\left(\kappa_{m,n,j}\right)\cos\xi_{m,n,j} + \sin c\left(\xi_{m,n,j}\right)\cos\kappa_{m,n,j}\right]$ $h_{m,n,j} = Ss_j\frac{2yc_j}{Ws_j}\cos\left(\frac{m\pi}{Lb}xc_j\right)\sin c\left(\frac{m\pi}{Lb}Ls_j\right)\sin c\left(\frac{n\pi}{Wb}yc_j\right)$ $sg_j = 1$ if the isosceles triangular is oriented as fig. (a) $sg_j = -1$ if the isosceles triangular is oriented as fig. (b)	(21)

Two specific error metrics named ΔT_s and $\overline{\Delta T_s}$ are fixed for evaluating the agreement of the model, as reported in eq. (22). The numerical results are considered as the reference value:

$$\Delta T_s = \frac{T_{\text{AM}} - T_{\text{NM}}}{T_{\text{NM}} - T_\infty} \quad \text{or} \quad \overline{\Delta T_s} = \frac{\overline{T_{\text{AM}}} - \overline{T_{\text{NM}}}}{\overline{T_{\text{NM}}} - T_\infty} \tag{22}$$

Board physical geometries

The current study deals with a standardized JEDEC vehicle test board, defined as high effective thermal conductivity test board. This one can be compared to an industrial PCB frame with its external signal traces on the component sides and its two internal power-ground planes of 35 μm. It is commonly described as a 2s2p board.

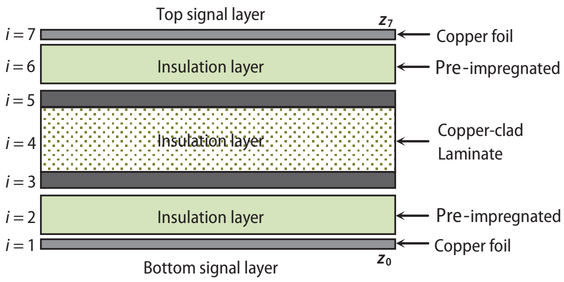

Figure 3. The 2s2p laminated cross-section overview

Therefore a 2s2p board is a stack-up of seven layers that alternates high and very low conductive layers, as shown in fig. 3.

The JEDEC JESD51 Standard details the requirements concerning the board size, thickness, dielectric material (FR-4) and traces width, length, and pitch. These parameters impact the amount of Cu and the capability of the PCB to spread the heat in-plane.

As a consequence, the effective thermal conductivity of the board layer stack-up is strongly anisotropic with a high heat spreading capability in-plane and a very poor one cross-plane. Their ratio is most of the time bigger than 50.

So right underneath the component, the thicknesses of the dielectric layers 2 and 6 have a major influence on the way the heat is removed. Their thickness was fixed at 250 μm which is the minimum value specified by JESD51-7. Metallization thicknesses of the top and bottom traces layers of the PCB were taken at 50 μm in order to compare the heat transfers to industrial realistic cases.

For the present study, the 2s2p board whose size is fixed at 75 × 100 × 1.6 mm was used as a test board.

Test board characteristics

Many theoretical and empirical models have been defined to estimate the effective thermal conductivity of a composite solid mixture [18]. Moreover, when the source PCB size ratio is below 0.1, the conventional concept of a homogenous single layer model that lumped the layers of the board must be given up [19] and the *N*-layer structure kept.

For the current study, the effective thermal conductivities of the PCB structure are based on the calculation models:

Sigmoidal model (s) $$K_{*,i}^{s} = \phi_{*,i} K_{*,i}^{u} + \left(1 - \phi_{*,i}\right) K_{*,i}^{l} \tag{23}$$

Upper model (u) $$K_{*,i}^{u} = \phi_{*,i} kf + \left(1 - \phi_{*,i}\right) km \tag{24}$$

Lower model (l) $$K_{*,i}^{l} = \frac{1}{4}\left(\gamma + \sqrt{\gamma^2 + 8kfkm}\right) \tag{25}$$

where

$$\gamma = \left(3\phi_{*,i} - 1\right)kf + \left[3\left(1-\phi_{*,i}\right) - 1\right]km \quad \text{and} \quad * = x \text{ or } y \text{ or } z \tag{26}$$

The parameters *km* and *kf* are, respectively, the thermal conductivities of the dielectric matrix and Cu filler and ϕ is the volume fraction of the filler. These values are fixed at 0.3 $Wm^{-1}K^{-1}$ for FR4 material and 400 $Wm^{-1}K^{-1}$ for the Cu.

Table 2 gives for the seven-layer 2s2p board the deducted effective thermal conductivities of each calculation models for the selected set of layer thicknesses and their Cu covering area factor.

Table 2. The 2s2p multi-layer thermal model data set

Layer *i*	t_i [μm]	$\phi_{*,i}$ [%]	$K^u_{x,i} = K^u_{y,i}$ [$Wm^{-1}K^{-1}$]	$K^l_{x,i} = K^l_{y,i}$ [$Wm^{-1}K^{-1}$]	$K^s_{x,i} = K^s_{y,i}$ [$Wm^{-1}K^{-1}$]	$K^u_{z,i}$ [$Wm^{-1}K^{-1}$]
7	50	15	60.3	0.5	9.5	60.3
6	250	0	0.3	0.3	0.3	0.3
5	35	95	380	370	379.5	380
4	930	0	0.3	0.3	0.3	0.3
3	35	95	380	370	379.5	380
2	250	0	0.3	0.3	0.3	0.3
1	50	15	60.3	0.5	9.5	60.3

The grey columns are used for modeling the thermal properties of the 2s2p multi-layered structure.

Pertinence of the proposed analytical approach

Three test cases were investigated in order to confirm the relevance of the proposed analytical formulae. The 2s2p board was submitted to the following laboratory boundary conditions:
– both upper and lower heat transfer coefficients *(ht, hr)* at 12.2 W/m^2K, and
– a reference temperature fixed at $T_\infty = 85$ °C,

The comparison between the models has been done on the center and average temperatures of each board layer considering the planar source having various shapes, locations or sizes.

Test case 1. Oriented square source

A 45 degree oriented square source is mounted at the center of the top surface of the 2s2p test board. The source size varies from 1 mm to 10 mm. A uniform heat power dissipation of 0.25 W is applied over the source.

In order to compare the Ansys© numerical results of this 45 degree oriented square source, the analytical model of two opposite isosceles triangles or one rhombus sources is assumed.

Table 3 shows the achieved good agreement between analytical and numerical calculations.

Figure 4 presents the centroid and mean temperature for several sizes of heating source.

This one demonstrates that both analytical models provide similar results and agreement to numerical simulations. Nevertheless, the use of superposition principle for two opposite

Table 3. Comparison of the predictions of the source temperatures

Source shape: Opposite isosceles triangles	Source $Ls \times Ws$ [mm²]	Analytical results		Numerical results		Error eq. (21)	
		Tc_{AM} [°C]	Tav_{AM} [°C]	Tc_{NM} [°C]	Tav_{NM} [°C]	ΔT_c [%]	ΔT_{av} [%]
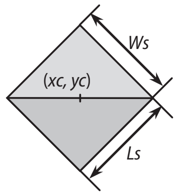	1 × 1	163.2	149.4	163.2	149.3	0.00	0.09
	2.5 × 2.5	116.9	110.6	116.8	110.6	0.04	0.06
	5 × 5	98.9	96.8	98.9	96.8	-0.01	0.06
	10 × 10	91.7	90.9	91.7	90.9	-0.04	0.07

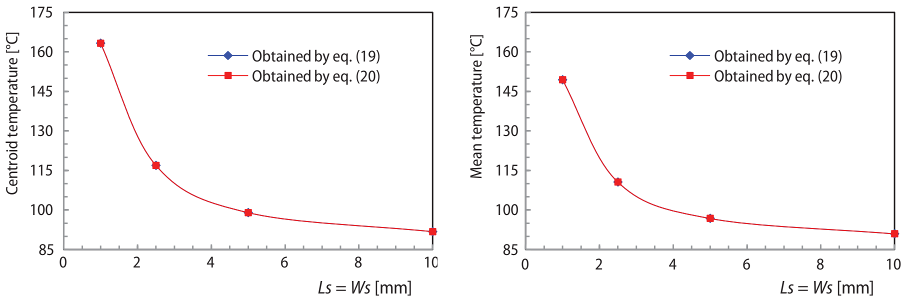

Figure 4. Comparison of temperature predictions of two opposite isosceles triangles and rhombus formulations

isosceles triangles model required more computation time to predict the temperatures. However, it can be noted that the analytical model is restricted to 45 degree rotated square sources.

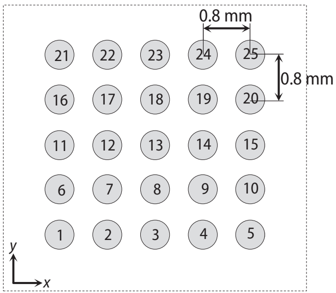

Figure 5. Configuration of the heating sources

Test case 2. Multiple identical heating sources

A set of 25 identical circular heating sources is placed at the center (xc = 37.5 mm, yc = 50 mm) of the front surface of 2s2p board, as shown in fig. 5.

Every source has a diameter of 0.6 mm and a uniform heat flux dissipation of 20 mW. The pitch between two sources in both x- and y-directions is equal to 0.8 mm. The nsx and nsy source numbers are equal to 5.

The temperatures of each source were determined from Bessel's formulae used for circular shape then compared to an Ansys© numerical simulation.

For this test case, the source temperature has been evaluated by two distinct ways:
- conventional superposition principle (8) and
- matrix-source solution (15).

The deducted results are identical and are presented, for centroid and mean temperatures, in tab. 4.

Table 5 highlights that the analytical results are compliant with the numerical results. The maximum temperature divergence is close to 0.05 °C. The error percentage for centroid or average temperature never exceeds to 0.1%.

Table 4. Comparison of the temperature predictions of the analytical and numerical models

Source number	Analytical results		Numerical results		Error eq. (22)	
	Tc_{AM} [°C]	Tav_{AM} [°C]	Tc_{NM} [°C]	Tav_{NM} [°C]	ΔT_{c} [%]	ΔT_{av} [%]
S1 – S5 – S21 – S25	112.21	111.02	112.19	111.00	0.07	0.08
S2 – S4 – S6 – S10 S16 – S20 – S22 – S24	116.07	114.98	116.05	114.96	0.06	0.07
S3 – S11 – S15 – S23	116.92	115.85	116.90	115.83	0.06	0.05
S7 – S9– S17 – S19	120.99	120.02	120.98	120.02	0.03	-0.01
S8 – S12 – S14 – S18	122.09	121.13	122.07	121.13	0.03	-0.01
S13	123.24	122.31	123.23	122.31	0.03	0.00

As mentioned previously, using the superposition principle requires more time to predict the temperature of all cylindrical sources. The compact matrix-source formula (15) offers a way to efficiently decrease the sum numbers and so the computation time. As a comparison, the Mathcad's computation time was reduced from 6 h and 30 min to 500 seconds per calculation.

Moreover, the multi-shaped heating source formulae allow us to quickly compare the temperature dissimilarity if the cylindrical shape of the source is replaced by a surface-equivalent square one, being able to be turned 45 degree, as drawn in fig. 6.

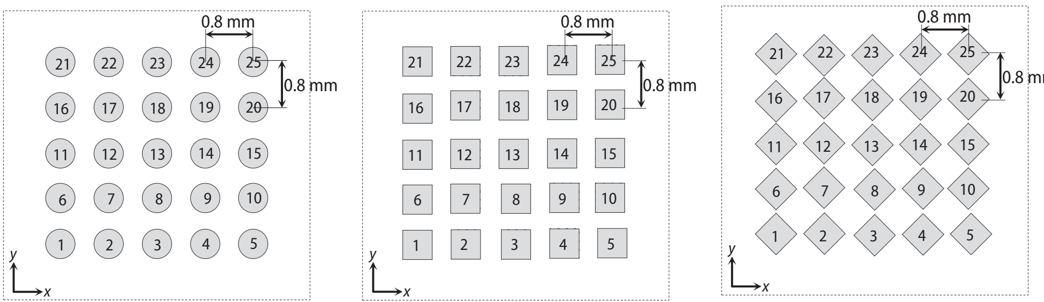

Figure 6. Studied arragements of the different shapes of heating sources

So the modeling of the cylindrical contacts of a Ball Grid Array component on an electronic board can be assumed to be surface-equivalent squares with no loss of precision.

Test case 3. Multi-shape heating sources

In a realistic application, there are always numerous heating sources with different shapes distributed all over the multi-layered PCB. Moreover, latest PCB technologies consider embedding components to reduce the size of the board assembly.

In the following case, a set of nine heat sources is mounted on the different layers of the 2s2p board as shown fig. 7.

Three among them are buried and located on the bottom of the upper 95% Cu layer, at z = 1.256 mm.

At the bottom board edges, four annular sources are assumed in contact with a cold-structure and as a consequence a fraction of the power dissipation is supposed drained

Table 5. Comparison of the temperature predictions for different shapes of sources

Source number	Centroid temperature [°C]			Average temperature [°C]		
	Cylindrical sources	Square sources	Oriented square sources	Cylindrical sources	Square sources	Oriented square sources
S1 – S5 – S21 – S25	112.21	112.15	112.17	111.03	110.94	110.98
S2 – S4 – S6 – S10 S16 – S20 – S22 – S24	116.07	116.01	116.04	114.98	114.89	114.94
S3 – S11 – S15 – S23	116.92	116.86	116.89	115.85	115.76	115.81
S7 – S9– S17 – S19	120.99	120.94	120.97	120.02	119.94	120.00
S8 – S12 – S14 – S18	122.09	122.03	122.06	121.13	121.05	121.11
S13	123.24	123.19	123.22	122.31	122.23	122.30

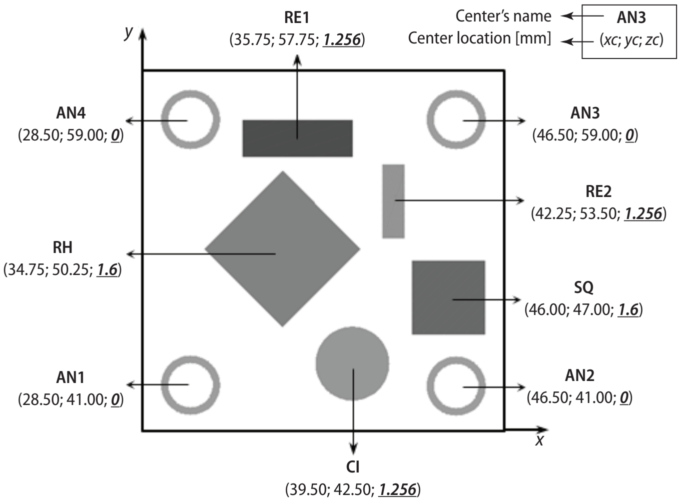

Figure 7. Distribution of different shape sources on the test board with their co-ordinates

from their area. The geometrical characteristics and power load of each source of the studied design are described in tab. 6.

Table 7 results enable to validate the pertinence of the developed analytical formulae by comparing the deducted results to the numerical calculation.

The agreement of the predictions of the local or the average temperature of each source is quite relevant. The divergence is lower than 0.2% whatever the source shape.

Table 6. List of the heating sources mounted on the board

Source shape	Name	Power [W]	Dimensions [mm]				Center location [mm]		
			Length (Ls)	Width (Ws)	Int. radius (R_i)	Ext. radius (R_e)	xc	yc	zc
Annular	AN1	–0.025	–	–	1.5	2	28.5	41	0
Annular	AN2	–0.025	–	–	1.5	2	46.5	41	0
Annular	AN3	–0.025	–	–	1.5	2	46.5	59	0
Annular	AN4	–0.025	–	–	1.5	2	28.5	59	0
Rectangular	RE1	0.2	7.5	2.5	–	–	35.75	57.75	1.256
Rectangular	RE2	0.1	1.5	5	–	–	42.25	53.5	1.256
Square	SQ	0.25	5	5	–	–	46	47	1.6
Rhombus	RH	0.5	7.5	7.5	–	–	34.75	50.25	1.6
Circular	CI	0.25	–	–	–	2.5	39.5	42.5	1.256

Conclusions

A Fourier's analytical model was completed in order to determine the steady-state temperature distribution of each layer of a multi-layer industrial board frame. The suggested

Table 7. Comparison of the temperature predictions of the analytical and numerical models

Source shape	Name	Analytical results		Numerical results		Error eq. (21)	
		Tc_{AM} [°C]	Tav_{AM} [°C]	Tc_{AM} [°C]	Tav_{AM} [°C]	ΔT_{c} [%]	ΔT_{av} [%]
Annular	AN1	93.9	93.2	93.2	93.2	–0.03	–0.12
Annular	AN2	948	94.1	94.1	94.1	–0.08	–0.15
Annular	AN3	94.2	93.4	93.4	93.4	–.012	–0.12
Annular	AN4	94.0	93.3	93.3	93.3	–0.04	–0.16
Rectangular	RE1	100.9	100.3	100.3	100.3	0.21	–0.16
Rectangular	RE2	101.3	101.0	101.1	101.1	0.19	–0.17
Square	SQ	108.8	106.7	106.7	106.7	0.11	–0.11
Rhombus	RH	110.6	108.5	108.5	108.5	–0.13	–0.13
Circular	CI	102.3	101.7	101.6	101.6	0.27	0.13

approach extends the use to multiple sources having various shapes which could be mounted on the in-plane external surfaces as well as embedded in its core structure.

The pertinence of a kit of practical expressions proposed for modeling board thermal behavior has been correlated from a set of electronics cooling software.

The agreement of the analytical modeling turns out quite relevant for early stages of a board design. The accuracy level and the computation time are compatible with industrial purposes.

Moreover, an optimal formulation applied to the case of multiple identical heating sources mounted on the PCB is supplied, this last one allowing shorter time calculation.

Further, the use of rhombus or opposite isosceles triangles allows us to characterize the behavior of 45 degree oriented square source.

However, the study shows the lack of an expression able to take into account the multiple orientations of heating source which are more and more encountered today in electronic board conception.

Nomenclature

A_m, B_n	– Fourier coefficients, [–]
$\overline{A_m}$, $\overline{B_n}$	– mean Fourier coefficients, [–]
hr, ht	– heat transfer coefficient, [Wm^{-2}K^{-1}]
K_x, K_y, K_z	– axis effective thermal conductivities, [Wm^{-1}K^{-1}]
kf	– thermal conductivities of Cu filler, [Wm^{-1}K^{-1}]
km	– thermal conductivities of dielectric matrix, [Wm^{-1}K^{-1}]
Lb, Wb, Hb	– the PCB dimensions, [m]
Ls, Ws, Hs	– source dimensions, [m]
M, N	– Fourier series truncation limit, [–]
nl, ns	– layers number, heating sources numbers, [–]
nsx, nsy	– axsial source number, [–]
px, py	– axial pitches, [m]
qs	– heating power, heat flow rate of source, [Wm^{-2}]
R	– radius of cylindrical sourse, [m]
Re, Ri	– internal and external radius of annular source, [m]
Sb, Ss	– the PCB and source area, [m^2]
T	– temperature, [K]
T_∞	– reference temperature, [K]
t	– layer thickness, [m]
xc, yc, zc	– center location of heating source, [m]
x, y, z	– local Cartesian co-ordinates, [m]

Greek symbols

δ	– Kronecker function
θ	– temperature excesses, [$= T(x,y,z) - T_\infty$], [K]
ω	– z-axis thermal profile
ϕ	– Cu coverage, [%]

Subscripts

i – layer identification
j – heating source identification
m, n – indices

Acronyms

AM, NM – analytical model, numerical model
PCB – printed circuit board

Appendix A

$$r_{m,n,i} = \sqrt{\left(\frac{m\pi}{Lb}\right)^2 \frac{Kx_i}{Kz_i} + \left(\frac{n\pi}{Wb}\right)^2 \frac{Ky_i}{Kz_i}} \tag{A.1}$$

$$\omega c_{m,n,i}(z) = 1 + \mathrm{e}^{-2zr_{m,n,i}} \quad \text{and} \quad \omega s_{m,n,i}(z) = \frac{1 - \mathrm{e}^{-2zr_{m,n,i}}}{r_{m,n,i}} \tag{A.2}$$

$$\alpha_{m,n,i} = kz_i r_{m,n,i}{}^2 \omega s_{m,n,i}(t_i) \tag{A.3}$$

$$\beta_{m,n,i} = (kz_i)^{-1} \omega s_{m,n,i}(t_i) \tag{A.4}$$

$$\gamma_{m,n,i} = \omega c_{m,n,i}(t_i) \tag{A.5}$$

$$Du_{m,n,i} = \alpha_{m,n,nl} + ht\beta_{m,n,nl}\chi u_{m,n,nl} + (\chi u_{m,n,nl} + ht)\gamma_{m,n,nl} \tag{A.6}$$

$$Nu_{m,n,i} = \frac{\mathrm{e}^{r_{m,n,nl}(z_{nl-1} - Hb)}}{\mathrm{e}^{r_{m,n,i}(z_{i-1} - Hb)}} \prod_{j=i}^{nl-1} \frac{2\mathrm{e}^{-t_j r_{m,n,j}}}{\gamma_{m,n,j} + \chi u_{m,n,j}\beta_{m,n,j}} \tag{A.7}$$

$$Dr_{m,n,i} = \alpha_{m,n,1} + hr\beta_{m,n,1}\chi l_{m,n,1} + (\chi l_{m,n,1} + hr)\gamma_{m,n,1} \tag{A.8}$$

$$Nr_{m,n,i} = \frac{\mathrm{e}^{-r_{m,n,1}z_1}}{\mathrm{e}^{-r_{m,n,i}(z_i + Hb)}} \prod_{j=i}^{2} \frac{2\mathrm{e}^{-t_j r_{m,n,j}}}{\gamma_{m,n,j} + \chi r_{m,n,j}\beta_{m,n,j}} \tag{A.9}$$

$$Deu_{m,n,i} = (\chi u_{m,n,s+1} + \chi r_{m,n,s})\left[\gamma_{m,n,s+1} + \chi r_{m,n,s+1}\beta_{m,n,s+1}\right] \tag{A.10}$$

$$Neu_{m,n,i} = \frac{\mathrm{e}^{-r_{m,n,s+1}t_{s+1}}}{\mathrm{e}^{-r_{m,n,i}(z_i + Hb)}} \prod_{j=i}^{s+2} \frac{2\mathrm{e}^{-t_j r_{m,n,j}}}{\gamma_{m,n,j} + \chi r_{m,n,j}\beta_{m,n,j}} \tag{A.11}$$

$$Der_{m,n,i} = (\chi u_{m,n,s+1} + \chi r_{m,n,s})\left[\gamma_{m,n,s} + \chi u_{m,n,s}\beta_{m,n,s}\right] \tag{A.12}$$

$$Ner_{m,n,i} = \frac{\mathrm{e}^{-r_{m,n,s}t_s}}{\mathrm{e}^{r_{m,n,i}(z_{i-1} - Hb)}} \prod_{j=i}^{s-1} \frac{2\mathrm{e}^{-t_j r_{m,n,j}}}{\gamma_{m,n,j} + \chi u_{m,n,j}\beta_{m,n,j}} \tag{A.13}$$

Appendix B

$$A_{m,j}B_{n,j} = \int_{xc_j - R_j}^{xc_j + R_j} \int_{yc_j - \sqrt{R_j^2 - (x - xc_j)^2}}^{yc_j + \sqrt{R_j^2 - (x - xc_j)^2}} \cos\left(\frac{m\pi}{Lb}x\right)\cos\left(\frac{n\pi}{Wb}y\right)\mathrm{d}x\mathrm{d}y \tag{B.1}$$

Reference

[1] Funk, J. N., *et al.*, A Semi-Analytical Method to Predict Printed Circuit Board Package Temperatures, *IEEE Transactions on Components*, *Hybrids and Manufacturing Technology*, *15* (1992), 5, pp. 675-684

[2] Ellison, G. N., Extensions of the Closed form Method for Substrate Thermal Analysers to Include Thermal Resistances from Source-to-Substrate and Source-to-Ambient, *IEEE Transactions on Components, Hybrids and Manufacturing technology*, *15* (1992), 5, pp. 658-666

[3] Chien, D. H. *et al.*, Temperature Solution of Five-Layer Structure with a Circular Embedded Source and its Application, *IEEE Transactions on Components, Hybrids and Manufacturing Technology*, *15* (1992), 5, pp. 707-714

[4] Rinaldi, N., Generalized Image Method with Application to the Thermal Modelling of Power Devices and circuits, *IEEE Transactions on Electron Devices*, *49* (2002), 4, pp. 679-686

[5] Albers, J., An Exact Recursion Relation Solution for the Steady-State Surface Temperature of a General Multilayer structure, *IEEE Transactions on Components, Packaging and Manufacturing Technology*, *18* (1995), 1, pp. 31-38

[6] Bagnall, K. R., *et al.*, Analytical Thermal Model for HEMTS with Complex Epitaxial Structures, *Proceedings*, The Intersociety Conference on Thermal and Thermo Mechanical Phenomena in Electronic Systems (ITHERM), Cupertino, Cal, USA, 2014

[7] Culham, J. R., *et al.*, Thermal Characterization of Electronic Package Using a Three-Dimensional Fourier Series Solution, *Journal of Electronic Packaging*, *122* (2000), 3, pp 233-239

[8] Ditri, J., Heat Conduction in Microwave Devices with Orthotropic and Temperature-Dependent Thermal Conductivity, *IEEE Transactions on Microvawe Theory and Techniques*, *55* (2007), 3, pp. 555-560

[9] Vintrou, S., *et al.*, Calculation and Analysis of Thermal Impedance of Microelectronic Structures from Analytical Models, *Solid-State Electronics*, *67*, (2012), 1, pp. 45-52

[10] Sadeghi, E., *et al.*, Thermal Spreading of Arbitrary-Shape Heat Source on a Half-Space: a Unified Approach, *IEEE Transactions on Components and Packaging Technologies*, *33* (2010), 2, pp. 267-277

[11] Hristov, J., An Alternative Integral-Balance Solution to Transient Diffusion of Heat (Mass) by Time-Fractional Semi-Derivatives and Semi-Integrals: Fixed Boundary Conditions, *Thermal Science*, *20* (2016), 6, pp. 1967-1978

[12] Fabre, A., Hristov, J., On the Integral-Balance Approach to the Transient Heat Conduction with Linearly Temperature-Dependent Thermal Diffusivity, *Heat Mass Transfer*, *7* (2017), 1, pp. 177-204

[13] Maranzana, G., *et al.*, Quasi-Analytical Simulation of Conduction Heat Transfer through a Pyramidal Multilayer Multiblock by the Quadrupole Method, *Numerical Heat Transfer*, *Part B, 42,* (2002), 6, pp 499-521

[14] Pailhes, J., *et al.*, Thermal Quadrupole Method with Internal Heat Sources, *International Journal of Thermal Sciences*, *53*, (2012), Mart, pp. 49-55

[15] Monier-Vinard, E., *et al.*, Analytical Thermal Modeling of Multi-Layered Active Embedded Chips into High Density Electronic Board, *Thermal Science*, *17* (2013), 3, pp. 695-706

[16] Monier-Vinard, E., *et al.*, Analytical Modeling of Multi-Layered Printed Circuit Board Dedicated to Electronic Component Thermal Characterization, *Solid State Electronic Journal*, *103* (2015), Jan., pp. 30-39

[17] Laraqi, N., Thermal Resistance for Random Contacts on the Surface of a Semi-Infinite Heat Flux Tube, *Journal of Heat Transfer*, *125* (2003), pp. 532-535

[18] Pabst, W., Gregorova, E., The Sigmoidal Average – A Powerful Tool for Predicting the Thermal Conductivity of Composite Ceramics, 6th European Thermal Sciences Conference, Poitiers, France, 2012

[19] Nguyen, M-N., *et al.*, Calculation Limits of Homogeneous Effective Thermal Conductivity Approach in Modeling of PCB, *Proceedings*, 20th Therminic Conference, London, 2014

Paper submitted: April 16, 2016
Paper revised: May 24, 2016
Paper accepted: June 15, 2016